

# Essential role for autophagy protein Atg7 in the maintenance of axonal homeostasis and the prevention of axonal degeneration

Masaaki Komatsu<sup>\*†</sup>, Qing Jun Wang<sup>§¶</sup>, Gay R. Holstein<sup>¶</sup>, Victor L. Friedrich, Jr.<sup>¶</sup>, Jun-ichi Iwata<sup>\*†</sup>, Eiki Kominami<sup>†</sup>, Brian T. Chait<sup>§</sup>, Keiji Tanaka<sup>\*</sup>, and Zhenyu Yue<sup>¶||</sup>

<sup>¶</sup>Departments of Neurology and Neuroscience, Mount Sinai School of Medicine, New York, NY 10029; <sup>\*</sup>Laboratory of Frontier Science, Tokyo Metropolitan Institute of Medical Science, Bunkyo-ku, Tokyo 113-8613, Japan; <sup>†</sup>Department of Biochemistry, Juntendo University School of Medicine, Bunkyo-ku, Tokyo 113-8421, Japan; <sup>‡</sup>Precursory Research for Embryonic Science and Technology, Japan Science and Technology Corporation, Kawaguchi 332-0012, Japan; and <sup>§</sup>Laboratory of Mass Spectrometry and Gaseous Ion Chemistry, Rockefeller University, New York, NY 10065

Edited by Pietro V. De Camilli, Yale University School of Medicine, New Haven, CT, and approved July 19, 2007 (received for review February 14, 2007)

**Autophagy is a regulated lysosomal degradation process that involves autophagosome formation and transport. Although recent evidence indicates that basal levels of autophagy protect against neurodegeneration, the exact mechanism whereby this occurs is not known. By using conditional knockout mutant mice, we report that neuronal autophagy is particularly important for the maintenance of local homeostasis of axon terminals and protection against axonal degeneration. We show that specific ablation of an essential autophagy gene, *Atg7*, in Purkinje cells initially causes cell-autonomous, progressive dystrophy (manifested by axonal swellings) and degeneration of the axon terminals. Consistent with suppression of autophagy, no autophagosomes are observed in these dystrophic swellings, which is in contrast to accumulation of autophagosomes in the axonal dystrophic swellings under pathological conditions. Axonal dystrophy of mutant Purkinje cells proceeds with little sign of dendritic or spine atrophy, indicating that axon terminals are much more vulnerable to autophagy impairment than dendrites. This early pathological event in the axons is followed by cell-autonomous Purkinje cell death and mouse behavioral deficits. Furthermore, ultrastructural analyses of mutant Purkinje cells reveal an accumulation of aberrant membrane structures in the axonal dystrophic swellings. Finally, we observe double-membrane vacuole-like structures in wild-type Purkinje cell axons, whereas these structures are abolished in mutant Purkinje cell axons. Thus, we conclude that the autophagy protein *Atg7* is required for membrane trafficking and turnover in the axons. Our study implicates impairment of axonal autophagy as a possible mechanism for axonopathy associated with neurodegeneration.**

axon | axonopathy | neurodegeneration | autophagosome | Purkinje cell

**M**acroautophagy is characterized by dynamic membrane rearrangements, involving the formation, trafficking, and degradation of double-membrane autophagic vacuoles (autophagosomes) in the cytoplasm. Macroautophagy (hereafter referred to as autophagy) is a highly regulated process, which can be induced by nutrient starvation, trophic factors, and stress (1). Despite recent advances in characterizing autophagy in several model systems, autophagic processes in the nervous system remain poorly understood. On one hand, nutrient deprivation has not been observed to induce autophagy in the mammalian brain (2), thus suggesting a specific regulatory system for autophagy that is not typically activated by starvation. On the other hand, a variety of conditions that cause neuronal stress or degeneration can lead to the accumulation of autophagosomes in neurons, thus implicating autophagy in these neuropathogenic processes (3, 4).

The axon is a highly specialized neuronal compartment that performs many functions independently from the cell body. After axotomy or excitotoxicity, double-membrane vacuoles

resembling autophagosomes were originally observed to accumulate in dilated axon terminals that result from the injury (5, 6), a local phenomenon that is not observed in undisturbed axons. Autophagosome-like vacuoles have also been shown to be present in the dysfunctional or degenerating axons associated with a range of chronic neurodegenerative conditions, including Alzheimer's (7, 8), Parkinson's (9), Huntington's (10), and Creutzfeldt–Jakob (11) diseases and their animal models (12–14). These observations suggest a link between locally altered autophagy and axonopathy, which is one of the underlying mechanisms in neurodegeneration (15).

Although the biological significance of these autophagosome-like vacuoles in degenerating axons is unclear, recent studies have shown that genetic inactivation of autophagy in the mouse CNS causes neurodegeneration accompanied by axonal dystrophy and the formation of intracellular ubiquitin-associated inclusions (16, 17). These studies suggest a role for basal levels of autophagy in neuronal protection and in protein quality control. However, the connection between the inactivation of autophagy and the observed axonal dystrophy and neurodegeneration remains to be determined. In addition, because autophagy was suppressed in all cell types in the CNS (including neurons and nonneuronal cells) (16, 17), it is not known whether the observed axonal dystrophy and neurodegeneration is cell-autonomous.

Here, we seek to further elucidate the physiological function of neuronal autophagy by generating conditional knockout mice with Purkinje cell-specific deletion of *Atg7*, an autophagy gene encoding E1-like enzyme in the two ubiquitin-like conjugation systems that are essential for the autophagosome biogenesis (18). We show that ablation of *Atg7* leads to abnormal swellings and dystrophy of Purkinje cell axon terminals in the deep cerebellar nuclei (DCN). Subsequently, these *Atg7*-deletion mice develop cell-autonomous neurodegeneration of Purkinje cells, dendritic atrophy, and behavioral deficits. Moreover, double-membrane vacuole-like structures are formed in the distal ends of wild-type Purkinje cell axons, whereas they are absent in *Atg7*-deletion Purkinje cell axons.

Author contributions: M.K. and Q.J.W. contributed equally to this work; M.K., Q.J.W., and Z.Y. designed research; M.K., Q.J.W., G.R.H., and J.-i.I. performed research; M.K., Q.J.W., G.R.H., V.L.F., J.-i.I., E.K., B.T.C., K.T., and Z.Y. analyzed data; and Q.J.W., B.T.C., and Z.Y. wrote the paper.

The authors declare no conflict of interest.

This article is a PNAS Direct Submission.

Abbreviations: DCN, deep cerebellar nucleus; Pn, postnatal day *n*; LC3, light chain 3; mGluR, metabotropic glutamate receptor.

<sup>||</sup>To whom correspondence should be addressed at: Department of Neurology, Mount Sinai School of Medicine, Box 1137, Annenberg 14-62, One Gustave L. Levy Place, New York, NY 10029. E-mail: zhenyu.yue@mssm.edu.

This article contains supporting information online at [www.pnas.org/cgi/content/full/0701311104/DC1](http://www.pnas.org/cgi/content/full/0701311104/DC1).

© 2007 by The National Academy of Sciences of the USA

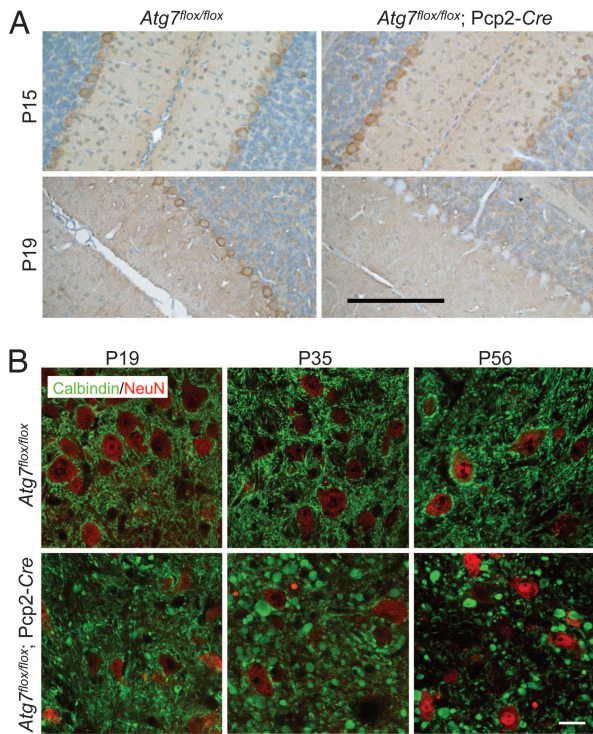


**Fig. 1.** Deletion of *Atg7* specifically in Purkinje cells caused progressive dystrophic swelling of axon terminals. (A) Immunohistochemistry of Atg7 protein expression in Purkinje cells of *Atg7<sup>fllox/fllox</sup>* and *Atg7<sup>fllox/fllox</sup>;Pcp2-Cre* mice at P15 and P19. The endogenous Atg7 protein was present at P15 but absent at P19 in the *Atg7<sup>fllox/fllox</sup>;Pcp2-Cre* Purkinje cells. (Scale bar: 100  $\mu$ m.) (B) Progression of the abnormal Purkinje cell axon terminal swellings in the DCN of *Atg7<sup>fllox/fllox</sup>;Pcp2-Cre* mice (anti-calbindin immunofluorescent staining in green with anti-NeuN counterstained in red) at P19, P35, and P56. *Atg7<sup>fllox/fllox</sup>* was used as control. (Scale bar: 20  $\mu$ m.)  $n = 3-5$ .

Instead, the mutant Purkinje cell axon terminal swellings accumulate aberrant membranous structures. Our results suggest that autophagy is required for normal axon terminal membrane trafficking and turnover, and indicate an essential role of local autophagy in the maintenance of axonal homeostasis and prevention of axonal degeneration.

## Results

**Specific Depletion of Atg7 in Purkinje Cells Caused Cell-Autonomous Dystrophy and Degeneration of Axon Terminals.** To generate Purkinje cell-specific deletion of *Atg7* in mice, we crossed mice harboring the floxed *Atg7* alleles (19) with transgenic mice expressing Cre recombinase under control of the *Pcp2* (L7) promoter (20) to establish the mouse line *Atg7<sup>fllox/fllox</sup>;Pcp2-Cre*. To determine when loss of the endogenous Atg7 protein occurred, we examined Atg7 expression in *Atg7<sup>fllox/fllox</sup>;Pcp2-Cre* mice at postnatal day 15 (P15) and P19. At P15, Atg7 was expressed at similar levels in Purkinje cells of both mutant *Atg7<sup>fllox/fllox</sup>;Pcp2-Cre* and the control *Atg7<sup>fllox/fllox</sup>* mice, whereas at P19, despite residual expression in a small number of Purkinje cells (<12%), Atg7 immunostaining was largely diminished in *Atg7<sup>fllox/fllox</sup>;Pcp2-Cre* Purkinje cells (>88%), but unchanged in the *Atg7<sup>fllox/fllox</sup>* Purkinje cells (Fig. 1A). At P35, >95% Purkinje cells in *Atg7<sup>fllox/fllox</sup>;Pcp2-Cre* showed no detectable Atg7 expression (data not shown). In addition, Atg7 deficiency in *Atg7<sup>fllox/fllox</sup>;Pcp2-Cre* mice was specific for Purkinje cells because Atg7 is clearly present in the other cell types (Fig. 1A). Thus, the specific loss of Atg7 in Purkinje cells occurred largely between P15 and P19 in *Atg7<sup>fllox/fllox</sup>;Pcp2-Cre* mice.

Next, we examined Purkinje cell axons in the DCN of

*Atg7<sup>fllox/fllox</sup>;Pcp2-Cre* mice by immunofluorescent staining using an antibody against calbindin, a Purkinje cell marker. At P15, no morphological alteration was observed in the axons of *Atg7<sup>fllox/fllox</sup>;Pcp2-Cre* Purkinje cells compared with those of *Atg7<sup>fllox/fllox</sup>* Purkinje cells [supporting information (SI) Fig. 7], consistent with the presence of normal levels of Atg7 in *Atg7<sup>fllox/fllox</sup>;Pcp2-Cre* Purkinje cells at this stage (Fig. 1A). However, at P19, *Atg7<sup>fllox/fllox</sup>;Pcp2-Cre* Purkinje cell axons were abnormally dilated, as visualized by green fluorescence-labeled “endbulbs” (Fig. 1B). In addition, these Purkinje cell axonal swellings were labeled with the antibody raised against synaptophysin, the presynaptic terminal marker (SI Fig. 8), suggesting that they were terminals of Purkinje cell axons. The number and size of the swollen axon terminals in the DCN of the *Atg7<sup>fllox/fllox</sup>;Pcp2-Cre* were markedly increased at P35 in comparison with those at P19 (Fig. 1B). At P56, the number of such axonal dystrophic swellings of the mutant Purkinje cells was noticeably decreased in comparison with that at P35, suggesting that many of these swollen axons had degenerated by this age (Fig. 1B). These data demonstrated that deletion of *Atg7* caused cell-autonomous axonal dystrophy and degeneration in Purkinje cells.

### Axonal Dystrophic Swellings of *Atg7<sup>fllox/fllox</sup>;Pcp2-Cre* Purkinje Cells Were Devoid of GFP-Light Chain 3 (LC3)-Labeled Puncta and Exhibited Increased Levels of p62/SQSTM1.

Transgenic mice producing GFP fused with microtubule-associated protein 1 light chain 3 (LC3), a specific marker for autophagosomes (21), were previously generated to monitor autophagosomes *in vivo* (2). By expressing GFP-LC3 in *Lurcher* mice (GFP-LC3/*Lurcher*), we showed that a large number of autophagosomes were formed in the dystrophic axon terminals of *Lurcher* Purkinje cells (Fig. 2Ad), providing *in vivo* evidence for the induction of autophagy in response to *Lurcher*-induced excitotoxicity (22). To assess autophagic activity in the dystrophic axons of *Atg7<sup>fllox/fllox</sup>;Pcp2-Cre* Purkinje cells, we crossed transgenic GFP-LC3 with *Atg7<sup>fllox/fllox</sup>;Pcp2-Cre* mice (*Atg7<sup>fllox/fllox</sup>;Pcp2-Cre*/GFP-LC3). Despite intense GFP-LC3 accumulation in the axonal dystrophic swellings of Purkinje cells in *Atg7<sup>fllox/fllox</sup>;Pcp2-Cre*/GFP-LC3 mice at P35, no GFP-LC3 fluorescent puncta characteristic of autophagosomes were observed in these swellings (Fig. 2A b and c). We contrasted this finding to our observation of GFP-LC3 puncta in Purkinje cell axons GFP-LC3/*Lurcher* mice (Fig. 2Ad) (22). In addition, no GFP-LC3 puncta were observed in the somata or dendrites of *Atg7<sup>fllox/fllox</sup>;Pcp2-Cre*/GFP-LC3 Purkinje cells (Fig. 2A f and g), again in contrast to the observation of GFP-LC3 puncta in the somata and dendrites of GFP-LC3/*Lurcher* Purkinje cells (Fig. 2Ah) (22).

It has been shown that inhibition of autophagy is correlated with increased levels of the polyubiquitin binding protein p62/SQSTM1 (22, 23). We thus examined the levels of p62/SQSTM1 in *Atg7<sup>fllox/fllox</sup>;Pcp2-Cre* Purkinje cells. As detected with anti-p62/SQSTM1 immunofluorescent staining, p62/SQSTM1 was markedly accumulated in the axonal dystrophic swellings (Fig. 2B, arrows) and somata (SI Fig. 9) of *Atg7<sup>fllox/fllox</sup>;Pcp2-Cre* Purkinje cells in comparison with *Atg7<sup>fllox/fllox</sup>* Purkinje cells. It is also noteworthy that the dystrophic axonal swellings in *Lurcher* Purkinje cells did not have detectable p62/SQSTM1 immunofluorescent staining (SI Fig. 10). These results provided molecular evidence for impaired autophagic activity in the dystrophic axons of *Atg7<sup>fllox/fllox</sup>;Pcp2-Cre* Purkinje cells, but not in the dystrophic axons of *Lurcher* Purkinje cells.

### *Atg7<sup>fllox/fllox</sup>;Pcp2-Cre* Purkinje Cells Exhibited Normal Dendritic Tree and Spine Morphology at P56.

Despite the remarkable dystrophy and degeneration of Purkinje cell axon terminals in the DCN of *Atg7<sup>fllox/fllox</sup>;Pcp2-Cre* mice at P35 and P56, the cerebellar cortex displayed little change in its overall size and organization (Fig. 3A). For example, at P35 and P56, *Atg7<sup>fllox/fllox</sup>;Pcp2-Cre* mice and

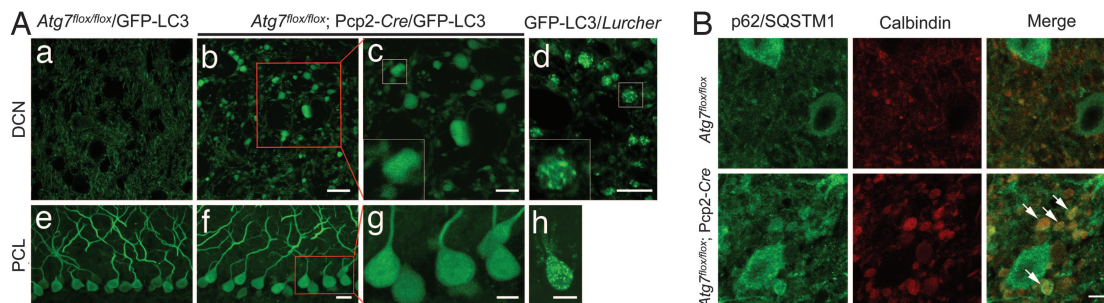


**Fig. 2.** The axonal dystrophic swellings of the *Atg7*-deficient Purkinje cells contained no GFP-LC3 labeled autophagosomes but accumulated p62/SQSTM1. (A) The absence of GFP-LC3 puncta in Purkinje cell axonal dystrophic swellings (*b* and *c*) and somata (*f* and *g*) of *Atg7<sup>lox/flox</sup>;Pcp2-Cre/GFP-LC3* mice (P35). GFP-LC3 puncta were found in GFP-LC3/*Lurcher* Purkinje cell axonal dystrophic swellings (*d*) and somata (*h*) (P12). DCN (*a*) and Purkinje cell layer (PCL) (*e*) of control mice *Atg7<sup>lox/flox</sup>/GFP-LC3* are shown. (Scale bars: *a*, *b*, *e*, and *f*, 20  $\mu$ m; *c*, *d*, *g*, and *h*, 10  $\mu$ m.) (B) Anti-p62/SQSTM1 immunofluorescent staining (in green) showed accumulation of p62/SQSTM1 in Purkinje cell axonal dystrophic swellings (calbindin labeling in red) (white arrows) in the DCN of *Atg7<sup>lox/flox</sup>;Pcp2-Cre* mice at P56. *Atg7<sup>lox/flox</sup>* was used as control. (Scale bar: 10  $\mu$ m.)

*Atg7<sup>lox/flox</sup>* mice did not exhibit significant difference in their cerebellar molecular layer thickness (Fig. 3*A* and *B*). To evaluate changes in dendritic tree and spine morphology, we examined the expression pattern of metabotropic glutamate receptor 1 $\alpha$  (mGluR1 $\alpha$ ) protein, a marker for parallel fiber–Purkinje cell synapses. No difference in localization and intensity of the anti-mGluR1 $\alpha$  immunofluorescent staining was observed between the *Atg7<sup>lox/flox</sup>;Pcp2-Cre* and *Atg7<sup>lox/flox</sup>* cerebellar molecular layers at either P35 (data not shown) or P56 (Fig. 3*C*). Thus, *Atg7* deletion had little effect on Purkinje cell dendritic tree and spine morphology up to at least P56. We conclude that *Atg7*

deletion in Purkinje cells elicit differential effects on the dendritic and axonal compartments, suggesting that the axon terminals are particularly vulnerable to autophagy deficiency.

**Axonal Dystrophy Preceded Cell-Autonomous Degeneration of Purkinje Cells and Behavioral Deficits in *Atg7<sup>lox/flox</sup>;Pcp2-Cre* Mice.** To further evaluate the effects of *Atg7* deletion, we assayed for Purkinje cell degeneration and mouse behavioral deficits. Whereas the Purkinje cell axonal dystrophic swellings in the DCN of *Atg7<sup>lox/flox</sup>;Pcp2-Cre* mice first became apparent at P19 and grew severe at P35 (Fig. 2*A*), no significant difference in Purkinje cell numbers was observed between the *Atg7<sup>lox/flox</sup>;Pcp2-Cre* and *Atg7<sup>lox/flox</sup>* mice at both ages (Fig. 4*A* and *B*). However, at P56, the number of Purkinje cells in *Atg7<sup>lox/flox</sup>;Pcp2-Cre* mice was reduced by 28.4% ( $P < 0.0005$ ) compared with *Atg7<sup>lox/flox</sup>* mice (Fig. 4*A* and *B*). Thus, loss of Purkinje cells in *Atg7<sup>lox/flox</sup>;Pcp2-Cre* mice occurred between P35 and P56. In comparison, the onset of axonal dystrophy began as early as P19. In addition, levels of GluR $\delta$ 2 (a Purkinje cell-specific glutamate receptor subtype) in *Atg7<sup>lox/flox</sup>;Pcp2-Cre* cerebellar extract were not reduced until P56 (SI Fig. 11), further supporting that the onset of axon dystrophy was earlier than Purkinje cell degeneration in *Atg7<sup>lox/flox</sup>;Pcp2-Cre* mice.

Next, we assessed the locomotive behaviors in *Atg7<sup>lox/flox</sup>;Pcp2-Cre* mice by limb-clasping, rotarod, and gait analyses at different postnatal ages. At P19 and P35, *Atg7<sup>lox/flox</sup>;Pcp2-Cre* mice appeared normal and did not show any difference in performance compared with their control *Atg7<sup>lox/flox</sup>* littermates (data not shown). At P56, *Atg7<sup>lox/flox</sup>;Pcp2-Cre* and *Atg7<sup>lox/flox</sup>* mice performed equally well on the rotarod and gait analyses (Fig. 4*C* and *D*). However, 5 of 13 *Atg7<sup>lox/flox</sup>;Pcp2-Cre* mice (38.5%) displayed limb-clasping reflexes on tail suspension, in comparison with 0 of 10 of their control littermates ( $P < 0.01$ ). Thus, at P56, despite the 28.4% loss of Purkinje cells (Fig. 4*B*), *Atg7<sup>lox/flox</sup>;Pcp2-Cre* mice displayed only mild behavioral impairment. In contrast, at 1 year, these mice demonstrated severe behavioral disorders in locomotion and motor coordination when evaluated in all three behavioral tests (Fig. 4*C* and *D*; data not shown).

We summarize the temporal relationship of the morphological alterations, differential pathology in different compartments of Purkinje cells, and behavioral changes in *Atg7<sup>lox/flox</sup>;Pcp2-Cre* mice in SI Table 1. These results demonstrate that axonal dystrophic swelling is an early pathogenic event and is likely to be a direct result of impairment of local autophagy in axon terminals.

**Aberrant Membrane Structures Accumulated in the Dystrophic Axon Terminals of *Atg7<sup>lox/flox</sup>;Pcp2-Cre* Purkinje Cells.** To further assess the effect of impairment of autophagy on axon terminals, we characterized the axonal dystrophic swellings of *Atg7<sup>lox/flox</sup>;Pcp2-Cre*

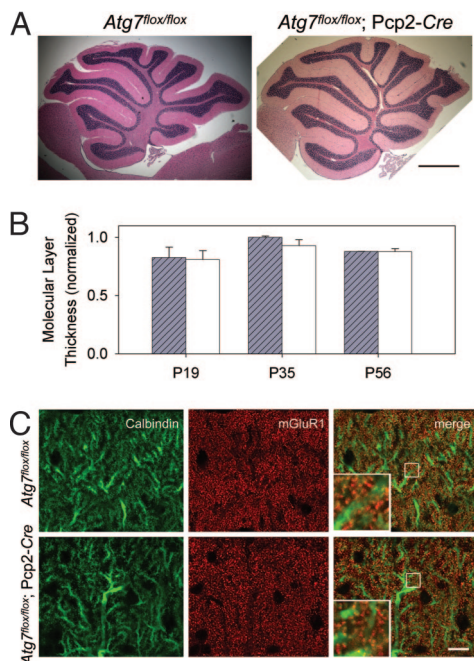


**Fig. 3.** Deletion of *Atg7* in Purkinje cells had little effect on the morphology of cerebellar cortex, Purkinje cell dendritic tree and spines in *Atg7<sup>lox/flox</sup>;Pcp2-Cre* mice at P56. (A) H&E-stained images of mid-sagittal sections from *Atg7<sup>lox/flox</sup>* and *Atg7<sup>lox/flox</sup>;Pcp2-Cre* cerebella at P56. (Scale bar: 0.5 mm.)  $n = 3-5$ . (B) Quantification of the molecular layer thickness (as the distance between lobules V and VI of the Purkinje cell layer divided by 2) from the cerebellar mid-sagittal sections of *Atg7<sup>lox/flox</sup>* and *Atg7<sup>lox/flox</sup>;Pcp2-Cre* mice at P19, P35, and P56.  $n = 3-5$ . (C) Immunofluorescent staining of cerebellar mid-sagittal sections shows normal localization and appearance of mGluR1 $\alpha$  (in red) in *Atg7<sup>lox/flox</sup>;Pcp2-Cre* mice compared with *Atg7<sup>lox/flox</sup>* mice at P56. Green indicates anti-calbindin. (Scale bar: 10  $\mu$ m.)  $n = 3$ .

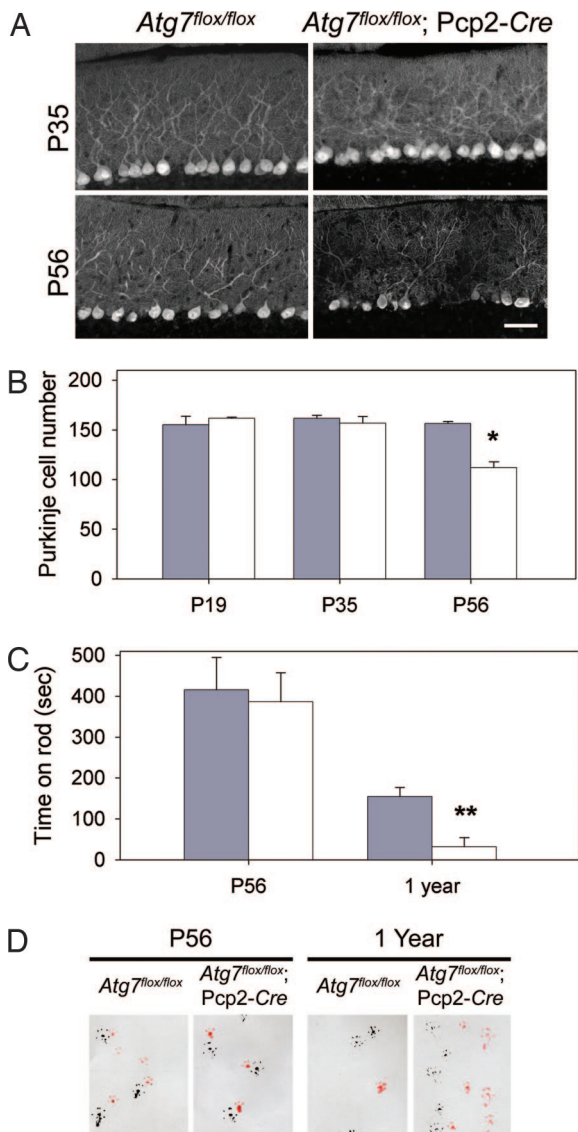


**Fig. 4.** Time course of Purkinje cell degeneration and locomotive behavioral deficits in *Atg7<sup>lox/flox</sup>;Pcp2-Cre* mice. (A) Anti-calbindin immunofluorescent staining of the cerebellar mid-sagittal sections of *Atg7<sup>lox/flox</sup>* and *Atg7<sup>lox/flox</sup>;Pcp2-Cre* mice at P35 and P56. (B) Quantitation of Purkinje cells at lobules IV–V of the mid-sagittal sections of *Atg7<sup>lox/flox</sup>* and *Atg7<sup>lox/flox</sup>;Pcp2-Cre* mice at P19, P35, and P56 based on H&E-stained images.  $n = 3, 3,$  and  $3$  for *Atg7<sup>lox/flox</sup>* at P19, P35, and P56, respectively.  $n = 2, 3,$  and  $5$  for *Atg7<sup>lox/flox</sup>;Pcp2-Cre* at P19, P35, and P56, respectively (\*,  $P < 0.0005$ ). (C) At P56, *Atg7<sup>lox/flox</sup>* and *Atg7<sup>lox/flox</sup>;Pcp2-Cre* mice showed no significant difference in the time spent on the rod in rotarod assay. At 1 year, *Atg7<sup>lox/flox</sup>* mice spent much longer time on the rod than *Atg7<sup>lox/flox</sup>;Pcp2-Cre* mice (\*\*,  $P < 0.05$ ). (D) In-gait analyses at P56, *Atg7<sup>lox/flox</sup>* and *Atg7<sup>lox/flox</sup>;Pcp2-Cre* mice showed similar step width and overlapping of forefeet and hindfeet (forefeet, red; hindfeet, black). At 1 year old, *Atg7<sup>lox/flox</sup>;Pcp2-Cre* mice showed shorter step width than *Atg7<sup>lox/flox</sup>* mice as well as nonoverlapping forefeet and hindfeet (left feet, black; right feet, red). For both C and D,  $n = 5$  at P56;  $n = 3$  and  $4$  at 1 year.

*Cre* Purkinje cells by transmission electron microscopy. The cross-sections of the Purkinje cell axon terminals in the DCN of the *Atg7<sup>lox/flox</sup>* mice were normally  $0.5\text{--}2\ \mu\text{m}$  in diameter (Fig. 5A, white arrows). Remarkably, the swollen Purkinje cell axon terminals in the DCN of the *Atg7<sup>lox/flox</sup>;Pcp2-Cre* mice often spanned  $1\text{--}6\ \mu\text{m}$  in diameter (Fig. 5B–F, black arrows) and differed profoundly in their morphology from the axonal dystrophic swellings observed in *Lurcher* Purkinje cells (Fig. 5G,

black arrows). The Purkinje cell axonal dystrophic swellings of *Lurcher* mice contained a large number of autophagosomes/autolysosomes (Fig. 5G), whereas those of the *Atg7<sup>lox/flox</sup>;Pcp2-Cre* mice were devoid of autophagosomes (Fig. 2 and 6Af). However, these autophagosome-free swellings of the *Atg7<sup>lox/flox</sup>;Pcp2-Cre* Purkinje cell axons often contained abnormal organelles or membrane structures (Fig. 5B–F, white arrows), including stacks of cisternal membranes that formed lamellar bodies (Fig. 5B and E, white arrows) (24), large and elaborate cisternal arrays and filaments (Fig. 5F, white arrow), and highly convoluted double-membrane whorls that occupied  $1.5\text{--}2\ \mu\text{m}$  of the swollen terminal (Fig. 5C and D, white arrows). The exact nature of these aberrant structures was not clear; they were rarely seen in the somata of *Atg7<sup>lox/flox</sup>;Pcp2-Cre* Purkinje cells (data not shown) or in the *Atg7<sup>lox/flox</sup>* Purkinje cells axons (Fig. 5A). However, it is noteworthy that the formation of convoluted membrane whorls was previously described in hepatocytes with *Atg7* deletion and was attributed to a failure in autophagic degradation (19). Our observations suggest a conserved function for autophagy in the clearance of cellular membranes and/or lipids in both axon terminals and hepatocytes.

**Vacuole-Like Structures with Double Membranes Were Formed in Normal Purkinje Cell Axons but Were Absent in the Dystrophic Axon Terminals of *Atg7<sup>lox/flox</sup>;Pcp2-Cre* Purkinje Cells.** Interestingly, through further ultrastructural analysis, we observed vacuole-like structures with double membranes in the myelinated Purkinje cell axons in the DCN of control *Atg7<sup>lox/flox</sup>* mice (Fig. 6Aa and SI Fig. 12). These structures typically appeared to be closed and had diameters of  $0.1\text{--}0.5\ \mu\text{m}$  (Fig. 6Aa). We occasionally observed these double-membrane vacuole-like structures in the process of formation (Fig. 6A b–e and SI Fig. 12A). Many of these developing double-membrane vacuole-like structures appeared to be formed through invagination of the axolemma along the myelinated layers (Fig. 6A b and c, SI Fig. 12A), reminiscent of invasion by oligodendrocytic processes (25, 26). Some of them appear to be continuous with the axonal plasma membrane (Fig. 6A d and e), which are enwrapping portions of axoplasm (27). The average number of these distinct double-membrane vacuole-like structures (both closed and in the process of formation) in Purkinje cell axons of *Atg7<sup>lox/flox</sup>* mice was  $\approx 0.9/50\ \mu\text{m}^2$  (Fig. 6B). In contrast, these structures were virtually absent in the *Atg7<sup>lox/flox</sup>;Pcp2-Cre* mice (Fig. 6Af, B, and C). Although we have yet to determine the exact nature of the vacuole-like structures with double membranes and their relationship with autophagosomes, our results suggested that *Atg7* was required for the formation of these distinct structures in axon terminals of normal Purkinje cells.

## Discussion

Axonal dystrophic swelling is a hallmark of CNS axonopathy, which can be triggered by neuronal injuries, excitotoxicity, and various neurodegenerative conditions. Despite the prevalence of this pathology, the molecular mechanisms underlying axonopathy as well as the connection between axonopathy and neurodegeneration remain poorly understood (28). A critical question is whether axonal dystrophy and degeneration precede neuronal cell death or are secondary to neurodegeneration. Here, we analyzed the time course of pathological events after the deletion of the autophagy gene *Atg7* in cerebellar Purkinje cells. We showed that axonal dystrophy and degeneration caused by ablation of *Atg7* occurred much earlier than the onset of neuronal death, indicating that axonal dystrophy was not secondary to neurodegeneration. In addition, axonal dystrophy and degeneration was a cell-autonomous event, which precluded the action of glia as the primary cause of the axonal dystrophy in *Atg7<sup>lox/flox</sup>;Pcp2-Cre* mice. Although this study was limited to Purkinje cells for the purpose of cell type-specific study of autophagy, axonal dystrophies occurred widely in many



normally participate in the formation of these structures. Thus, we hypothesize that, in addition to the role in protein quality control (16, 17), neuronal autophagy regulates membrane homeostasis in the axon terminals. Furthermore, we showed that deletion of *Atg7* caused the axonal terminal swelling, which was a reminiscence of hepatic cell swelling in *Atg7*-deleted mouse liver (19). It is conceivable that axon terminals and hepatocytes may share a similar mechanism for cell (or cellular compartment) size control, which requires autophagy (31).

Previous morphological studies have consistently shown the presence of large numbers of autophagosome-like vacuoles in axonal dystrophic swellings of injured neurons (4–13). We have previously demonstrated that induction of autophagy in *Lurcher* Purkinje cells involved accumulation of autophagosomes in the dystrophic axons (22). In contrast, our present study shows that the axonal swellings of Purkinje cells in *Atg7<sup>lox/flox</sup>;Pcp2-Cre* mice were devoid of vacuoles that resembled the autophagosomes observed in *Lurcher* mice. Although our present study demonstrates a role for basal levels of autophagy in axonal protection and indicates that altered autophagy could serve as an adaptive response for remodeling the axon terminals for regeneration (3, 22), we cannot exclude the possibility that up-regulation of autophagy in dystrophic axons is actually destructive, causing overdegradation of axonal structures. This possibility can be tested, in principle, by genetic crossing of the autophagy-deficient mice with diseased mice containing the autophagosome-like vacuoles in dystrophic axons or cell bodies.

In summary, our study provides genetic and molecular evidence for the indispensable role of neuronal autophagy in the maintenance of axonal homeostasis, particularly in local membrane trafficking and turnover. Perturbation of local autophagy in the axons leads to axonopathy. We believe that it is important to study the connection between axonal autophagy impairment and human neuropathological conditions associated with axonal dystrophy.

## Materials and Methods

**Antibodies.** Antibodies used were mouse monoclonal anti-calbindin D-28K (Swant, Bellinzona, Switzerland), anti-calbindin (Sigma, St. Louis, MO), anti-GluR $\delta$ 2 (BD Transduction Laboratories, San Diego, CA), anti-p62 (American Research Products, Belmont, MA), Cy3-conjugated anti-mouse and anti-rabbit IgG (Upstate Biotechnology, Lake Placid, NY), and NeuN, mGluR $\alpha$ , and actin antibodies (Chemicon International, Temecula, CA). Anti-*Atg7* is described in ref. 19.

**Animals.** *Pcp2-Cre* transgenic mice (20) (The Jackson Laboratory, Bar Harbor, ME) and *Atg7<sup>lox/flox</sup>* mice (19) were crossed to produce *Atg7<sup>lox/flox</sup>;Pcp2-Cre* mice. *Atg7<sup>lox/flox</sup>;Pcp2-Cre* mice and GFP-LC3 transgenic mice (2) were crossed to produce *Atg7<sup>lox/flox</sup>;Pcp2-Cre*/GFP-LC3 mice.

**Histological Examination.** Mice were fixed by cardiac perfusion with 0.1 M phosphate buffer containing 4% paraformaldehyde. The color images of the Meyer's H&E-stained midsagittal cryosections (10  $\mu$ m) of cerebella were acquired with a 20 $\times$  objective lens and a color CCD camera, and later assembled to full images in Photoshop for the quantification of Purkinje cells. Immunofluorescent stained cerebellar samples were prepared as described in ref. 22 and examined by using confocal microscopy.

**Behavioral Analyses.** Motor function was assessed by the limb-clasping test, rotarod assay, and gait analysis (*SI Materials and Methods*).

**Electron Microscopy.** Tissue samples were obtained from three *Atg7<sup>lox/flox</sup>* mice and three *Atg7<sup>lox/flox</sup>;Pcp2-Cre* mice. Details of the experiment are described in *SI Materials and Methods*. In brief, thin sections (70 nm) of the lateral cerebellar nucleus and cerebellar cortex were prepared and examined by transmission electron microscopy (H7500; Hitachi, Tokyo, Japan). A double-blind point-counting method was used to quantify double-membrane vacuole-like structures in 55 micrographs of either *Atg7<sup>lox/flox</sup>* or *Atg7<sup>lox/flox</sup>;Pcp2-Cre* mice. The total number of these structures overlying at least one intersection of a Photo-shop-generated grid was counted to be 52 and 13 for *Atg7<sup>lox/flox</sup>* and *Atg7<sup>lox/flox</sup>;Pcp2-Cre* samples, respectively. The total number of intersections within these structures was 132 and 19 for *Atg7<sup>lox/flox</sup>* and *Atg7<sup>lox/flox</sup>;Pcp2-Cre* samples, respectively.

**Statistical Analyses.** The equality of the variance was first tested by using the *F* test. Pair-wise comparisons were calculated by using one-tailed Student's *t* test. The standard error was calculated for each sample.

We thank X. Li, Y. Ding, T. Kouno, and K. Tatsumi for excellent technical assistance; A. North in the Rockefeller Bio-Imaging Resource Center for help with microscopy; and S. Waguri, T. Ueno, I. Tanida, J. Ezaki, and N. Heintz for helpful discussion. This study was supported by National Institutes of Health Grants RNS055683A (to Z.Y.), RR00862, and RR022220 (both to B.T.C.).

- Levine B, Klionsky DJ (2004) *Dev Cell* 6:463–477.
- Mizushima N, Yamamoto A, Matsui M, Yoshimori T, Ohsumi Y (2004) *Mol Biol Cell* 15:1101–1111.
- Rubinsztein DC, DiFiglia M, Heintz N, Nixon RA, Qin ZH, Ravikumar B, Stefanis L, Tolkovsky A (2005) *Autophagy* 1:11–22.
- Yue Z, Horton A, Bravin M, DeJager PL, Selimi F, Heintz N (2002) *Neuron* 35:921–933.
- Dixon JS (1967) *Nature* 215:657–658.
- Matthews MR, Raisman G (1972) *Proc R Soc Lond Ser B* 181:43–79.
- Nixon RA, Wegiel J, Kumar A, Yu WH, Peterhoff C, Cataldo A, Cuervo AM (2005) *J Neuropathol Exp Neurol* 64:113–122.
- Cataldo AM, Hamilton DJ, Barnett JL, Paskevich PA, Nixon RA (1996) *J Neurosci* 16:186–199.
- Anglade P, Vyas S, Javoy-Agid F, Herrero MT, Michel PP, Marquez J, Mouatt-Prigent A, Ruberg M, Hirsch EC, Agid Y (1997) *Histol Histopathol* 12:25–31.
- Roizin L, Stellar S, Willson N, Whittier J, Liu JC (1974) *Trans Am Neurol Assoc* 99:240–243.
- Sikorska B, Liberski PP, Giraud P, Kopp N, Brown P (2004) *Int J Biochem Cell Biol* 36:2563–2573.
- Yu WH, Cuervo AM, Kumar A, Peterhoff CM, Schmidt SD, Lee JH, Mohan PS, Mercken M, Farmery MR, Tjernberg LO, et al. (2005) *J Cell Biol* 171:87–98.
- Lin WL, Lewis J, Yen SH, Hutton M, Dickson DW (2003) *J Neurocytol* 32:1091–1105.
- Li H, Li SH, Yu ZX, Shelbourne P, Li XJ (2001) *J Neurosci* 21:8473–8481.
- Coleman MP, Perry VH (2002) *Trends Neurosci* 25:532–537.
- Komatsu M, Waguri S, Chiba T, Murata S, Iwata J, Tanida I, Ueno T, Koike M, Uchiyama Y, Kominami E, et al. (2006) *Nature* 441:880–884.
- Hara T, Nakamura K, Matsui M, Yamamoto A, Nakahara Y, Suzuki-Migishima R, Yokoyama M, Mishima K, Saito I, Okano H, et al. (2006) *Nature* 441:885–889.
- Ohsumi Y, Mizushima N (2004) *Semin Cell Dev Biol* 15:231–236.
- Komatsu M, Waguri S, Ueno T, Iwata J, Murata S, Tanida I, Ezaki J, Mizushima N, Ohsumi Y, Uchiyama Y, et al. (2005) *J Cell Biol* 169:425–434.
- Barski JJ, Dethleffsen K, Meyer M (2000) *Genesis* 28:93–98.
- Kabeya Y, Mizushima N, Ueno T, Yamamoto A, Kirisako T, Noda T, Kominami E, Ohsumi Y, Yoshimori T (2000) *EMBO J* 19:5720–5728.
- Wang QJ, Ding Y, Kohtz S, Mizushima N, Cristea IM, Rout MP, Chait BT, Zhong Y, Heintz N, Yue Z (2006) *J Neurosci* 26:8057–8068.
- Bjorkoy G, Lamark T, Brech A, Outzen H, Perander M, Overvatn A, Stenmark H, Johansen T (2005) *J Cell Biol* 171:603–614.
- Banno T, Kohno K (1998) *J Comp Neurol* 402:252–263.
- Zhang P, Land W, Lee S, Juliani J, Lefman J, Smith SR, Germain D, Kessel M, Leapman R, Rouault TA, et al. (2005) *J Struct Biol* 150:144–153.
- Eddleman CS, Ballinger ML, Smyers ME, Fishman HM, Bittner GD (1998) *J Neurosci* 18:4029–4041.
- Li YC, Li YN, Cheng CX, Sakamoto H, Kawate T, Shimada O, Atsumi S (2005) *Neurosci Res* 53:298–303.
- Coleman M (2005) *Nat Rev Neurosci* 6:889–898.
- Broadwell RD, Cataldo AM (1984) *J Comp Neurol* 230:231–248.
- Hollenbeck PJ (1993) *J Cell Biol* 121:305–315.
- Hosokawa N, Hara Y, Mizushima N (2006) *FEBS Lett* 580:2623–2629.